Available online at www.sciencedirect.com
SCIENCE DIRECT®
International Journal of Heat and Mass Transfer 47 (2004) 307–328
International Journal of HEAT and MASS TRANSFER
www.elsevier.com/locate/ijhmt

Volumetric interfacial area prediction in upward bubbly two-phase flow

Wei Yao [1], Christophe Morel *

CEA Grenoble, DEN/DTP/SMTH/LMDS, 17 rue des Martyrs, 38054 Grenoble, Cédex 9, France

Received 28 May 2002; received in revised form 13 June 2003

Abstract

In two-phase flow studies, a volumetric interfacial area balance equation is often used in addition to the multi-dimensional two-fluid model to describe the geometrical structure of the two-phase flow. In the particular case of bubbly flows, numerous works have been done by different authors on the subject. Our work concerns two main modifications of this balance equation: (1) new time scales are proposed for turbulence induced coalescence and breakup, (2) modeling of the nucleation of new bubbles on the volumetric interfacial area. The 3D module of the CATHARE code is used to evaluate our new model, in comparison to three other models for interfacial area found in the literature, on two different experiments. First, we use the DEBORA experimental data base for the comparison in the case of *boiling* bubbly flow. The comparison of the different volumetric interfacial area models to the DEBORA experimental data shows that even though the theoretical values of the coefficients are adopted in our modified model, this model has a quite good capability to predict the local two-phase geometrical parameters in the boiling flow conditions. Secondly, we compare the predictions obtained with the same models to the DEDALE experimental data base, for the case of *adiabatic* bubbly flow. In comparison to the other models tested, our model also gives quite good predictions of the bubble diameter in the case of adiabatic conditions.

Keywords: Boiling two-phase flow; Interfacial area; Nucleation; Bubbly flow; DEBORA experiment; DEDALE experiment

1. Introduction and discussion about the volumetric interfacial area models

The two-fluid model is currently used in many general computational fluid dynamic codes and more specific nuclear thermal-hydraulics analysis codes, for two-phase flow studies. In the two-fluid model, the volumetric interfacial area, also called the interfacial area concentration, is a very important quantity which determines the intensity of inter-phase mass, momentum and energy transfers. As pointed out by Ishii [1], the accurate modeling of the local interfacial area concentration is the first step to be taken for the development of reliable two-fluid model closure relations. Recently, more and more researchers concentrate on developing the volumetric interfacial area transport equation to describe the temporal and spatial evolution of the two-phase geometrical structure.

As far as the adiabatic bubbly flow is concerned, the effects of nucleation and interfacial heat and mass transfers are out of consideration, thus the coalescence and breakup effects due to the interactions among bubbles and between bubbles and turbulent eddies have been the subject of more attention. Wu et al. [2] have considered five mechanisms responsible for bubbles coalescence and breakup: (1) coalescence due to random collisions driven by turbulence, (2) coalescence due to wake entrainment, (3) breakup due to the impact of turbulent eddies, (4) shearing-off of small bubbles from larger cap bubbles, (5) breakup of large cap bubbles due to interfacial instabilities. In the case of low void fraction conditions where no cap bubbles are present, the

* Corresponding author. Tel.: +33-4-38-78-92-27/56-54.
E-mail addresses: yao@alpes.cea.fr (W. Yao), morel@alpes.cea.fr (C. Morel).
[1] Tel.: +33-4-38-78-56-54.

0017-9310/$ - see front matter © 2003 Elsevier Ltd. All rights reserved.
doi:10.1016/j.ijheatmasstransfer.2003.06.004

Nomenclature

a_i	volumetric interfacial area
a_l	thermal diffusion coefficient of liquid
A	area
C	constant or coefficient
C_p	isobaric thermal capacity
d	diameter
e	internal energy
E	Zuber's factor for added mass (Eq. (85))
f	frequency, pdf
g	function given by Eq. (13), gravity
h	thickness, heat transfer coefficient, source term in Liouville equation
H	enthalpy
I	identity tensor
j	local volumetric flux
J	global volumetric flux (superficial velocity)
Ja	Jakob number
k	wave number
K	constant, turbulent kinetic energy
L	length, latent heat of vaporisation
m	gas mass in a bubble
$\dot{m}$	mass flux
M_{ki}	volumetric interfacial forces
n	bubble number density
n_e	mixture eddies number density
N	active nucleation sites number density, liquid eddies number density
Nu	Nusselt number
P	pressure
Pe	Péclet number
Pr	Prandtl number
P_K^i	bubble induced turbulence kinetic energy source term
P_ε^i	bubble induced turbulence dissipation rate source term
q	heat flux
q''	heat flux density
r	bubble radius
Re	Reynolds number
S	collision area
t	time
$\overleftrightarrow{t}$	stress tensor
T	period, temperature
u	turbulent velocity
U_r	norm of the relative velocity
V	volume
$\vec{V}$	velocity vector
We	Weber number
x	space coordinate
Z/D	elevation to tube diameter ratio in the DEDALE experiment

Greek symbols

α	void fraction
δ	Dirac distribution
δt	numerical time step
ε	turbulence dissipation rate
η	coalescence/breakup efficiency
ϕ	source/sink of bubble number density
ξ	internal phase coordinate
ψ	dispersed phase geometrical quantity
λ	thermal conductivity
ρ	density
τ	time constant
σ	surface tension
ν	viscosity
Δ	difference
Γ	interfacial mass transfer
Ω	variation domain for the internal phase coordinates

Superscripts

BK	breakup
CO	coalescence
D	drag
DT	turbulent dispersion
i	interfacial
L	lift
MA	added mass
NUC	nucleation
RC	random collision
Re	Reynolds
T	turbulence
TI	turbulent impact
WE	wake entrainment
+	non-dimensional (temperature)
$*$	friction (velocity)

Subscripts

0	initial value
b	breakup, bubble
bf	free travelling of breakup
bi	interaction of breakup
c	coalescence, continuous phase
cf	free travelling of coalescence
ci	interaction of coalescence
cr	critical value
d	dispersed phase
D	drag
DT	turbulent dispersion
e	eddy, evaporation
g	gas or vapour
i	interface
k	k-phase

ki	k-phase near the interface	q	quenching
K	relative to the turbulent kinetic energy	r	relative
l	liquid	s	Sauter mean (diameter)
L	lift	sat	saturation
max	maximum value	t	turbulent
MA	added mass	w	wall
nuc	nucleation	ε	relative to the turbulent dissipation rate

authors have simplified their model by considering only one bubble size and the first three coalescence and breakup mechanisms.

Some experimental results [3,4] show that the wake entrainment results in coalescence primarily between pairs of large cap bubbles in fluid sufficiently viscous to keep their wake laminar; whereas small spherical or ellipsoidal bubbles tend to repel each other. In addition, in low viscous liquids such as water, the turbulent wake has the tendency to break trailing bubbles because of its intermittency and irregularity. Hibiki and Ishii [5] also pointed out that the wake entrainment induced coalescence results in minor contribution to the volumetric interfacial area variation in the bubbly flow with high flow rate because a bubble captured in the wake region can leave the region easily due to liquid turbulence, even though it may play an important role in the bubbly-to-slug flow transition. Furthermore, calculation results of Hibiki and Ishii [5] and Ishii and Kim [6] have shown that the gas expansion term, previously omitted by Wu et al. [2], may contribute significantly to the total variation of volumetric interfacial area. In another hand, although the wake entrainment effect can be omitted for Hibiki, it appears dominant in Wu's calculation cases. In addition, although the coefficients are fitted from experimental data and can give reasonable one-dimensional calculation results, it is surprising to notice that the values presented by the different authors show significant differences. Recently, Delhaye [7] gave a systematic comparison and detailed analysis of their work.

The volumetric interfacial area transport equation written by the above authors writes:

$$\frac{\partial a_{\mathrm{i}}}{\partial t}+\nabla\cdot(a_{\mathrm{i}}\vec{V}_{\mathrm{g}})=\frac{2}{3}\frac{a_{\mathrm{i}}}{\alpha}\left[\frac{\partial\alpha}{\partial t}+\nabla\cdot(\alpha\vec{V}_{\mathrm{g}})\right]+\frac{36\pi}{3}\left(\frac{\alpha}{a_{\mathrm{i}}}\right)^{2}(\phi_n^{\mathrm{RC}}+\phi_n^{\mathrm{WE}}+\phi_n^{\mathrm{TI}}) \tag{1}$$

where the first term on the right-hand side (RHS) is the gas expansion term, and ϕ_n^{RC}, ϕ_n^{WE}, ϕ_n^{TI} are the volumetric bubble number variations induced by the coalescence and breakup phenomena. Clearly, the coalescence and breakup terms *induced by turbulence* can be written in the following general forms:

$$\phi_n^{\mathrm{RC}}=-\frac{1}{T_{\mathrm{c}}}n\eta_{\mathrm{c}},\quad \phi_n^{\mathrm{TI}}=\frac{1}{T_{\mathrm{b}}}n\eta_{\mathrm{b}} \tag{2}$$

where T_{c} and T_{b} are the coalescence and breakup times of a single bubble, η_{c} and η_{b} are the coalescence and breakup efficiencies, and n is the bubble number per unit volume. Table 1 shows a comparison of the models of different authors [2,5,6] according to our notations introduced in Eq. (2). In this table, the Weber number is defined by the following relation:

Table 1
Comparison of volumetric interfacial area models

Models	ϕ_n^{RC}		ϕ_n^{TI}		ϕ_n^{WE}	Expansion term
	T_{c}	η_{c}	T_{b}	η_{b}		
Wu et al. [2]	Free travelling time $\propto\frac{d_{\mathrm{s}}^{2/3}}{\varepsilon^{1/3}\alpha}g(\alpha)$	Constant	Interaction time $\propto\frac{d_{\mathrm{s}}}{u_{\mathrm{t}}}\left(1-\frac{We_{\mathrm{cr}}}{We}\right)^{-1/2}$	$\exp\left(-\frac{We_{\mathrm{cr}}}{We}\right)$	Yes	No
Hibiki and Ishii [5]	Free travelling time $\propto\frac{d_{\mathrm{s}}^{2/3}}{\varepsilon^{1/3}\alpha}g(\alpha)$	$\exp\left(-K_{\mathrm{c2}}\sqrt{\frac{We}{We_{\mathrm{cr}}}}\right)$	Free travelling time $\propto\frac{d_{\mathrm{s}}^{2/3}}{\varepsilon^{1/3}(1-\alpha)}h(\alpha)$	$\exp\left(-K_{\mathrm{B}}\frac{We_{\mathrm{cr}}}{We}\right)$	No	Yes
Ishii and Kim [6]	Free travelling time $\propto\frac{d_{\mathrm{s}}^{2/3}}{\varepsilon^{1/3}\alpha}g(\alpha)$	Constant	Interaction time $\propto\frac{d_{\mathrm{s}}}{u_{\mathrm{t}}}\left(1-\frac{We_{\mathrm{cr}}}{We}\right)^{-1/2}$	$\exp\left(-\frac{We_{\mathrm{cr}}}{We}\right)$	Yes	Yes

$$We = \frac{\rho_l u^2 d_s}{\sigma} = \frac{\text{inertial energy}}{\text{surface energy}} \tag{3}$$

and We_{cr} is a constant designated as the critical Weber number [2]. In a turbulent flow, if the bubble size is in the inertial subrange [8,9], the square of the velocity appearing in Eq. (3) is given by the following relation:

$$u^2 = 2.0(\varepsilon d_s)^{2/3} \tag{4}$$

where d_s is the (Sauter mean) bubble diameter and ε is the turbulent kinetic energy dissipation rate per unit mass of the continuous liquid phase. Therefore, we have:

$$We = \frac{2\rho_l(\varepsilon d_s)^{2/3} d_s}{\sigma} \tag{5}$$

It should be noted that Wu et al. [2] and Hibiki and Ishii [5] models are based on different methods to evaluate the time required for the bubbles breakup and coalescence (the model proposed by Ishii and Kim [6] is similar to the one proposed by Wu et al. [2] for the turbulence induced coalescence and breakup). For the breakup term, Wu et al. [2] evaluate the breakup time from a simplified momentum equation, considering only the interaction of a breaking bubble with a turbulent eddy of the same size. Therefore, we call this first time the 'interaction time'. Hibiki and Ishii [5] evaluate the breakup time as the time necessary for a given bubble to be collided by a turbulent eddy. We will call this second time the 'free travelling time'. It should be noted that the breakup time proposed by Hibiki and Ishii [5] is proportional to $(\alpha - \alpha_{max})$ where α_{max} is the 'maximum packing' value of the void fraction [1], therefore giving an infinite breakup frequency when $\alpha = \alpha_{max}$. In fact, the breakup frequency should be zero when $\alpha = \alpha_{max}$ because there is almost no liquid between the bubbles, and hence no turbulent eddies. The breakup model proposed by Wu et al. [2] does not consider the necessary free travelling time for a bubble to encounter a liquid eddy. Due to these shortcomings of the previous models, we will propose a new model in Section 2, for the turbulent breakup, taking into account the free travelling time and the interaction time separately.

For the coalescence term, Wu et al. [2] and Hibiki and Ishii [5] derived different characteristic times for binary collisions between bubbles from considerations about mean distance between neighbouring bubbles. Another important difference between their models is the coalescence efficiency retained by the different authors. Hibiki and Ishii [5] choose to model this coalescence efficiency as in Coulaloglou and Tavlaridès [10] for liquid/liquid dispersions, although Wu et al. [2] assume the coalescence efficiency to be constant. The time for liquid film drainage between two interacting bubbles can be quite long, giving smaller values for the coalescence efficiency. But this drainage time is also the time during which the two bubbles interact before to coalesce or to be separated by the turbulent eddies. We therefore propose a new model, given in Section 2, taking into account the time necessary for collision and the interaction time separately.

Another shortcoming in Wu et al. [2] and Ishii and Kim [6] models is that the breakup model they propose cannot be used for $We < We_{cr}$, due to the dependence in $\sqrt{1 - We_{cr}/We}$ (Table 1). These authors therefore assume that the bubble breakup is likely to occur only if:

$$We \geqslant We_{cr} \tag{6}$$

The significance of Eq. (6) is that only a turbulent eddy with sufficient energy to overcome the surface energy of the interacting bubble can break this bubble. However, as pointed out by Risso [9], turbulence acts on each bubble as a succession of colliding eddies, with random arrival times and intensities, instead of a single isolated eddy. If the frequencies of these successive eddies are close to the natural frequency of the bubble, the bubble shape may become to oscillate and these oscillations can break the bubble, even if $We < We_{cr}$. We have tried to take into account this resonance mechanism in the model we present in Section 2.

For the boiling two-phase flow conditions, a discussion of the nucleation contribution to the volumetric interfacial area is rarely found in previous papers. Kocamustafaogullari and Ishii [11] simply added the volumetric bubble number variation due to the nucleation ϕ_n^{NUC} in the corresponding balance equation. Therefore, the volumetric interfacial area balance equation (1) becomes:

$$\frac{\partial a_i}{\partial t} + \nabla \cdot (a_i \vec{V}_g) = \frac{2}{3}\frac{a_i}{\alpha}\left[\frac{\partial \alpha}{\partial t} + \nabla \cdot (\alpha \vec{V}_g)\right] + \frac{36\pi}{3}\left(\frac{\alpha}{a_i}\right)^2\left(\sum_j \phi_n^j + \phi_n^{NUC}\right) \tag{7}$$

No experimental results about the nucleation term can be found in their paper. Another aim of the present paper is to model the nucleation effect properly in the volumetric interfacial area transport equation. This aspect will be examined in Section 3 of our paper.

In Section 4, the other balance equations and closure relations we use to calculate the DEBORA and DEDALE experiments are briefly presented. In Sections 5 and 6, the calculations results we have obtained with the use of different interfacial area models are presented together with the experimental data, for DEBORA and DEDALE respectively. The results obtained with the different models are compared and discussed. Some conclusions and perspectives for future work are drawn in Section 7.

2. Modeling of the turbulence induced coalescence and breakup

As we discussed in the previous section, two main modifications of the turbulence induced coalescence and breakup models will be presented here:

(1) The times for coalescence and breakup can be split into two contributions: the free travelling time and the interaction time.
(2) The breakup interaction time is modeled according to the bubble-eddy resonance mechanism.

2.1. Turbulence induced coalescence

In a turbulent flow, small bubble motions are driven randomly by turbulent eddies. In the case where $d_s \ll L$, where d_s is the Sauter mean bubble diameter and L is the average distance between two neighbouring bubbles, the probability of collision between two bubbles is larger than the one among three or more bubbles. Assuming only binary coalescence events, Prince and Blanch [12] gave the following expression for the collision frequency between two bubbles of different groups induced by turbulence:

$$f_{ij}^{\mathrm{T}} = n_i n_j S_{ij} (u_i^2 + u_j^2)^{1/2} \tag{8}$$

where the effective collision cross-sectional area is given by:

$$S_{ij} = \frac{\pi}{4}(r_i + r_j)^2 \tag{9}$$

In the case of a single bubble size, given by d_s, the *total* collision frequency between bubbles in a unit volume can be simplified into:

$$f_c = \frac{\sqrt{2}\pi}{8} n^2 d_s^2 u = \frac{\pi}{4} n^2 d_s^{7/3} \varepsilon^{1/3} = C_c \frac{\varepsilon^{1/3}}{d_s^{11/3}} \alpha^2 \tag{10}$$

where $C_c = 2.86$. It should be noted that we have divided (8) by 2 for the calculation of the total collision frequency, in order to avoid double counting of the same collision events between bubble pairs [12].

Accordingly the average free travelling time of *one* bubble writes:

$$T_{cf} \triangleq \frac{n}{2 f_c} = \frac{4}{\sqrt{2}\pi n d_s^2 u} = \frac{1}{3} \frac{d_s^{2/3}}{\alpha \varepsilon^{1/3}} \tag{11}$$

It can be considered that when the void fraction reaches a certain value α_{max}, called 'maximum packing value' [1], the bubbles touch each other and the average free travelling time becomes zero. In the case of a single bubble size, this limiting value of the void fraction is given by [5]:

$$\alpha_{max} = \frac{\pi}{6} = 0.52 \tag{12}$$

Therefore, the following modification factor:

$$g(\alpha) = \frac{(\alpha_{max}^{1/3} - \alpha^{1/3})}{\alpha_{max}^{1/3}} \tag{13}$$

which considers the effect of the void fraction on the average free travelling time, is suggested here. When the void fraction is very small, $g(\alpha) = 1$, which corresponds to the case of a dilute two-phase flow where no correction is needed. If the void fraction reaches its limiting value, $g(\alpha) = 0$ and the free travelling time becomes nil.

At the end, the free travelling time can be expressed by the following relation:

$$T_{cf} = \frac{1}{3} \frac{g(\alpha)}{\alpha} \frac{d_s^{2/3}}{\varepsilon^{1/3}} \tag{14}$$

In the modeling of the interaction between two interacting bubbles, we adopt the film thinning model [13]. This model assumes that two bubbles will coalesce if the contact time between them, depending on the surrounding turbulent eddies, is larger than the liquid film drainage time. Prince and Blanch [12] gave the following expression for the film drainage time:

$$t_c = \left[\frac{\rho_c (d_s/2)^3}{16\sigma} \right]^{1/2} \ln \frac{h_0}{h_{cr}} \tag{15}$$

where the initial film thickness h_0 and the critical film thickness h_{cr} are suggested to be 10^{-4} m [13] and 10^{-8} m [14] (for an air–water system). Therefore, Eq. (15) can be rewritten:

$$t_c = 0.814 \sqrt{\frac{\rho_c d_s^3}{\sigma}} \tag{16}$$

This time is used as the interaction time before coalescence of two bubbles:

$$T_{ci} = t_c \tag{17}$$

The contact time is given by the characteristic time of the eddies having the same size than the bubbles [12]:

$$\tau_c = \frac{r_b^{2/3}}{\varepsilon^{1/3}} \tag{18}$$

In addition, an exponential relation is assumed [14] to estimate the collision efficiency:

$$\eta_c = \exp\left(-\frac{t_c}{\tau_c} \right) \tag{19}$$

As we discussed before, the coalescence time contains two parts: the free travelling time and the interaction time, i.e.:

$$T_c = T_{cf} + T_{ci} \tag{20}$$

Finally, the bubble coalescence frequency can be expressed as:

$$\phi_n^{\mathrm{RC}} = -\frac{1}{2}\frac{\eta_c n}{T_c} \tag{21}$$

where the factor one-half has been put to avoid double counting of the same coalescence events between bubble pairs [12].

Substituting from the above relations, the final form writes:

$$\phi_n^{\mathrm{RC}} = -K_{c1}\frac{\varepsilon^{1/3}\alpha^2}{d_s^{11/3}}\frac{1}{g(\alpha)+K_{c2}\alpha\sqrt{We/We_{cr}}} \times \exp\left(-K_{c3}\sqrt{\frac{We}{We_{cr}}}\right) \tag{22}$$

If we introduce the following value of the critical *Weber* number [15]:

$$We_{cr} = 1.24 \tag{23}$$

the coefficients will be $K_{c1} = 2.86$, $K_{c2} = 1.922$, $K_{c3} = 1.017$.

It should be noted that the ratio of the free travelling time and the interaction time is:

$$\frac{T_{cf}}{T_{ci}} \propto \frac{g(\alpha)}{\alpha\sqrt{We/We_{cr}}} \tag{24}$$

This time ratio decreases when the Weber number increases or the void fraction increases.

2.2. Turbulence induced breakup

For analysing the collisions between bubbles and eddies using Eq. (8), the information of eddies number per unit volume is needed. According to Azbel and Athanasios [16]:

$$\frac{\mathrm{d}N(k)}{\mathrm{d}k} = 0.1k^2 \tag{25}$$

where $N(k)$ is the number of eddies of wave number k per unit volume of the fluid ($k = 2/d_e$ where d_e is the diameter of the eddy).

Considering the void fraction effect, the number of eddies per unit volume in the two-phase mixture is given by [5]:

$$\frac{\mathrm{d}n_e(k)}{\mathrm{d}k} = 0.1k^2(1-\alpha) \tag{26}$$

which can be rewritten in terms of eddy diameter:

$$\mathrm{d}n_e(d_e) = \left| -0.8(1-\alpha)\frac{\mathrm{d}(d_e)}{d_e^4} \right| \tag{27}$$

Using Eqs. (4), (8), (9) and (27), the collision frequency between bubbles characterized by their volumetric number n and their diameter d_s and eddies whose diameters are comprised between two fixed values d_{e1} and d_{e2} is:

$$\begin{aligned} f_b &= \int_{d_{e1}}^{d_{e2}} n\frac{\pi}{16}(d_e+d_s)^2\sqrt{2}\varepsilon^{1/3}(d_e^{2/3}+d_s^{2/3})^{1/2}\,\mathrm{d}n_e(d_e) \\ &= \int_{d_{e1}}^{d_{e2}} (1-\alpha)n\frac{\pi}{16}(d_e+d_s)^2\sqrt{2}\varepsilon^{1/3}(d_e^{2/3}+d_s^{2/3})^{1/2}\frac{0.8}{d_e^4}\mathrm{d}(d_e) \end{aligned} \tag{28}$$

Assuming that only the eddies with a size comparable to the bubble diameter can break the bubbles, and numerically integrating Eq. (28) from $d_{e1} = 0.65d_s$ to $d_{e2} = d_s$ (the value 0.65 is chosen in order to obtain a good agreement on the bubble diameter profile in comparison to the DEBORA experiment), we obtain:

$$f_b = C_b'\frac{n\varepsilon^{1/3}}{d_s^{2/3}}(1-\alpha) = C_b\frac{\varepsilon^{1/3}}{d_s^{11/3}}\alpha(1-\alpha) \tag{29}$$

where $C_b = 6C_b'/\pi = 1.6$ ($C_b' = 0.837$).

Therefore, the average free travelling time of bubbles can be written as:

$$T_{bf} = \frac{n}{f_b} = C_{bt}\frac{d_s^{2/3}}{\varepsilon^{1/3}(1-\alpha)} \tag{30}$$

where $C_{bt} = 1/C_b' = 1.194$.

As pointed out previously, the breakup mechanism is assumed to be due to the resonance of bubble oscillations with turbulent eddies, especially in the conditions of low *Weber* number. The natural frequency of the nth order mode of the oscillating bubble is given by [9,13,15,17]:

$$(2\pi f_n)^2 = \frac{8n(n-1)(n+1)(n+2)\sigma}{[(n+1)\rho_g + n\rho_l]d_s^3} \tag{31}$$

For the second mode oscillation, and if $\rho_g \ll \rho_l$ is assumed for bubbly flow, Eq. (31) gives:

$$f_2 = 1.56\sqrt{\frac{\sigma}{\rho_l d_s^3}} \tag{32}$$

The breakup characteristic time describes the increase of the most unstable oscillation mode:

$$T_{bi} = \frac{1}{f_2} = 0.64\sqrt{\frac{\rho_l d_s^3}{\sigma}} \tag{33}$$

This characteristic time is used as the interaction time between a bubble and eddies. As for the coalescence, we assume that the breakup time is the sum of the free travelling time and the interaction time:

$$T_b = T_{bf} + T_{bi} \tag{34}$$

In addition, the breakup efficiency can be expressed as [2]:

$$\eta_b = \exp\left(-\frac{We_{cr}}{We}\right) \tag{35}$$

Finally, the bubble breakup frequency should be written as:

$$\phi_n^{\mathrm{TI}} = \eta_{\mathrm{b}} \frac{n}{T_{\mathrm{b}}} \tag{36}$$

Substituting from the above relations, the final form is obtained:

$$\phi_n^{\mathrm{TI}} = K_{\mathrm{b1}} \frac{\varepsilon^{1/3}\alpha(1-\alpha)}{d_{\mathrm{s}}^{11/3}} \frac{1}{1+K_{\mathrm{b2}}(1-\alpha)\sqrt{We/We_{\mathrm{cr}}}} \times \exp\left(-\frac{We_{\mathrm{cr}}}{We}\right) \tag{37}$$

where $K_{\mathrm{b1}} = 1.6$, $K_{\mathrm{b2}} = 0.42$.

The ratio of the free travelling time and the interaction time is given by the following relation:

$$\frac{T_{\mathrm{bf}}}{T_{\mathrm{bi}}} \propto \frac{1}{(1-\alpha)\sqrt{We/We_{\mathrm{cr}}}} \tag{38}$$

This ratio decreases when the Weber number increases or the void fraction decreases.

3. Modeling of the nucleation induced source term in the volumetric interfacial area transport equation

The volumetric interfacial area transport equation derived previously by other authors [2,5,6] is given by Eq. (1).

The mass balance equation for the gas phase can be written as:

$$\frac{\partial}{\partial t}(\alpha\rho_{\mathrm{g}}) + \nabla\cdot(\alpha\rho_{\mathrm{g}}\vec{V}_{\mathrm{g}}) = \Gamma_{\mathrm{g,i}} + \Gamma_{\mathrm{g,nuc}} \tag{39}$$

where the source term due to phase change has been split into two contributions: $\Gamma_{\mathrm{g,i}}$ and $\Gamma_{\mathrm{g,nuc}}$ are the interfacial mass transfer terms induced by *phase change without nucleation* and by *nucleation* respectively. Using the above equation, Eq. (1) can be rewritten as:

$$\frac{\partial a_{\mathrm{i}}}{\partial t} + \nabla\cdot(a_{\mathrm{i}}\vec{V}_{\mathrm{g}}) = \frac{2}{3}\frac{a_{\mathrm{i}}}{\alpha\rho_{\mathrm{g}}}\left[\Gamma_{\mathrm{g,i}} + \Gamma_{\mathrm{g,nuc}} - \alpha\frac{\mathrm{d}\rho_{\mathrm{g}}}{\mathrm{d}t}\right] + \frac{36\pi}{3}\left(\frac{\alpha}{a_{\mathrm{i}}}\right)^2(\phi_n^{\mathrm{RC}} + \phi_n^{\mathrm{WE}} + \phi_n^{\mathrm{TI}}) \tag{40}$$

The first term in the RHS includes the bubble size variations due to the mass transfer and to the gas expansion effect and the second term in the RHS represents the bubble number variations induced by coalescence and breakup. The two kinds of phase change, namely the nucleation part and the phase change through the surfaces of the existing bubbles, are considered together in Eq. (40). However, the nucleation generates many small newborn bubbles which give quite different contribution to the interfacial area concentration in comparison to the interfacial mass transfer through the surface of the existing bubbles. The question is: how to model the nucleation effect on the volumetric interfacial area properly? This question will be addressed in the two following subsections.

3.1. Method 1: derivation from the bubble number density equation

Let us introduce the bubble number source term per unit volume and time due to the nucleation ϕ_n^{NUC} in the following bubble number density equation:

$$\frac{\partial n}{\partial t} + \mathrm{div}(n\vec{V}_{\mathrm{g}}) = \phi_n^{\mathrm{NUC}} + \phi_n^{\mathrm{CO}} + \phi_n^{\mathrm{BK}} \tag{41}$$

where ϕ_n^{CO} and ϕ_n^{BK} are the bubble number density variations induced by coalescence and breakup respectively. Here, we have: $\phi_n^{\mathrm{CO}} = \phi_n^{\mathrm{RC}} + \phi_n^{\mathrm{WE}}$ and $\phi_n^{\mathrm{BK}} = \phi_n^{\mathrm{TI}}$.

Assuming a single bubble size given by the Sauter mean diameter, we have:

$$d_{\mathrm{s}} = \frac{6\alpha}{a_{\mathrm{i}}} \tag{42}$$

$$n = \frac{\alpha}{\pi d_{\mathrm{s}}^3/6} = \frac{1}{36\pi}\frac{a_{\mathrm{i}}^3}{\alpha^2} \tag{43}$$

Substituting Eq. (43) into Eq. (41), we obtain:

$$\frac{\partial a_{\mathrm{i}}}{\partial t} + \nabla\cdot(a_{\mathrm{i}}\vec{V}_{\mathrm{g}}) = \frac{2}{3}\frac{a_{\mathrm{i}}}{\alpha}\left[\frac{\partial\alpha}{\partial t} + \nabla\cdot(\alpha\vec{V}_{\mathrm{g}})\right] + \frac{36\pi}{3}\left(\frac{\alpha}{a_{\mathrm{i}}}\right)^2(\phi_n^{\mathrm{NUC}} + \phi_n^{\mathrm{CO}} + \phi_n^{\mathrm{BK}}) \tag{44}$$

This equation has been written by [2,5]. Using Eq. (39), Eq. (44) can be rewritten as:

$$\frac{\partial a_{\mathrm{i}}}{\partial t} + \nabla\cdot(a_{\mathrm{i}}\vec{V}_{\mathrm{g}}) = \frac{2}{3}\frac{a_{\mathrm{i}}}{\alpha\rho_{\mathrm{g}}}\left[\Gamma_{\mathrm{g,i}} + \Gamma_{\mathrm{g,nuc}} - \alpha\frac{\mathrm{d}\rho_{\mathrm{g}}}{\mathrm{d}t}\right] + \frac{36\pi}{3}\left(\frac{\alpha}{a_{\mathrm{i}}}\right)^2(\phi_n^{\mathrm{NUC}} + \phi_n^{\mathrm{CO}} + \phi_n^{\mathrm{BK}}) \tag{45}$$

Assuming that all the nucleated bubbles appear with the diameter d_{s}, their total contribution to the volumetric interfacial area is:

$$\pi d_{\mathrm{s}}^2\phi_n^{\mathrm{NUC}} \equiv 36\pi\left(\frac{\alpha}{a_{\mathrm{i}}}\right)^2\phi_n^{\mathrm{NUC}} \tag{46}$$

It should be noted that the nucleation term proportional to ϕ_n^{NUC} in the RHS of Eq. (45) given by:

$$\frac{36\pi}{3}\left(\frac{\alpha}{a_{\mathrm{i}}}\right)^2 \phi_n^{\mathrm{NUC}} \tag{47}$$

is only one third of the total nucleation term given by Eq. (46). In the other hand, we can rewrite the nucleation part in the first term of the RHS of Eq. (45) into the following manner:

$$\begin{aligned}\frac{2}{3}\frac{a_{\mathrm{i}}}{\alpha\rho_{\mathrm{g}}}\Gamma_{\mathrm{g,nuc}} &= \frac{2}{3}\frac{a_{\mathrm{i}}}{\alpha\rho_{\mathrm{g}}}\phi_n^{\mathrm{NUC}}\rho_{\mathrm{g}}\frac{\pi d_{\mathrm{s}}^3}{6}\\ &= \frac{2}{3}36\pi\left(\frac{\alpha}{a_{\mathrm{i}}}\right)^2\phi_n^{\mathrm{NUC}}\end{aligned} \tag{48}$$

which gives the two other thirds of the nucleation term.

We see that the nucleation part of the volumetric interfacial area transport equation, as derived by several authors on the assumption of a single bubble size [2,5,6], is split into two terms. A first term, proportional to the bubble number density source term, contains only one third of the total variation of the volumetric interfacial area due to nucleation. The two other thirds are contained in the term proportional to the void fraction variation. We prefer reunify these two terms into a single one in order to treat the nucleation and the remaining part of the phase change separately. This will allow us to introduce some information about the diameter of the newly nucleated bubbles, which is smaller than the Sauter mean diameter d_{s}.

3.2. Method 2: derivation from the so-called Liouville equation

The population of the bubbles in the flow can be described by using a probability density function (pdf). This pdf denoted by $f(\xi,x,t)$ is governed by the so-called Liouville equation. This equation writes [18]:

$$\frac{\partial f}{\partial t} + \mathrm{div}[f\dot{x}(\xi,x,t)] + \sum_{j=1}^{n}\frac{\partial f\dot{\xi}_j}{\partial\xi_j} = h(\xi,x,t) \tag{49}$$

where the quantities ξ_j are some parameters describing the bubbles, called 'internal phase coordinates'. The third term in the left-hand side (LHS) of Eq. (49) corresponds to effect of the time rate of change of the quantities ξ_j measured along each bubble path and the RHS of Eq. (49) represents a generalised bubble source term.

Multiplying Eq. (49) by a given function $\psi(\xi,x,t)$ characterising the dispersed phase and integrating, we obtain:

$$\begin{aligned}&\frac{\partial}{\partial t}\int_\Omega \psi f\,\mathrm{d}\xi + \mathrm{div}\int_\Omega \psi\dot{x}f\,\mathrm{d}\xi\\ &\quad= \int_\Omega \psi h\,\mathrm{d}\xi + \sum_{j=1}^{n}\int_\Omega \dot{\xi}_j\frac{\partial\psi}{\partial\xi_j}f\,\mathrm{d}\xi + \int_\Omega\left(\frac{\partial\psi}{\partial t}+\dot{x}\cdot\nabla\psi\right)f\,\mathrm{d}\xi\end{aligned} \tag{50}$$

where Ω is the domain of variations of the internal phase coordinates ξ_j.

It can be written:

$$\frac{\mathrm{d}\psi(\xi,x,t)}{\mathrm{d}t} = \frac{\partial\psi}{\partial t} + \sum_{j=1}^{3}\frac{\partial\psi}{\partial x_j}\frac{\mathrm{d}x_j}{\mathrm{d}t} + \sum_{j=1}^{n}\frac{\partial\psi}{\partial\xi_j}\frac{\mathrm{d}\xi_j}{\mathrm{d}t} \tag{51}$$

which is the material derivative of the quantity ψ. This material derivative corresponds to the time rate of change of ψ measured along each bubble path. Finally, Eq. (50) can be rewritten as:

$$\begin{aligned}&\frac{\partial}{\partial t}\int_\Omega \psi f\,\mathrm{d}\xi + \mathrm{div}\int_\Omega \psi\dot{x}f\,\mathrm{d}\xi\\ &\quad= \int_\Omega \psi h\,\mathrm{d}\xi + \int_\Omega \frac{\mathrm{d}\psi}{\mathrm{d}t}f\,\mathrm{d}\xi\end{aligned} \tag{52}$$

3.2.1. Bubble number density equation

If we assume that the bubbles are spherical, it is sufficient for our purpose to consider only one parameter ξ, namely the bubble diameter d. In this context, the bubble number density is defined by:

$$n \equiv \int_\Omega f\,\mathrm{d}(d) \tag{53}$$

and the averaged velocity transporting this bubble number density is defined by:

$$\vec{V}_n \equiv \frac{\int_\Omega \dot{x}f\,\mathrm{d}(d)}{\int_\Omega f\,\mathrm{d}(d)} \tag{54}$$

The total bubble number density source term is defined by:

$$\phi_n = \int_\Omega h\,\mathrm{d}(d) \tag{55}$$

Considering the three above definitions, the bubble number density transport equation can be obtained by making $\psi = 1$ in Eq. (52). We obtain:

$$\frac{\partial n}{\partial t} + \mathrm{div}(n\vec{V}_n) = \phi_n \tag{56}$$

It must be noted that the RHS of the bubble number density transport equation (56) represents only the bubble number changes, and not the changes in size or shape of the bubbles. Eq. (56) is the same as Eq. (41) if we assume that the velocity $\mathbf{V}_n$ can be well approximated by the averaged gas velocity $\mathbf{V}_{\mathrm{g}}$.

3.2.2. Volumetric interfacial area transport equation

Now we take $\psi = A = \pi d^2$ which is the interfacial area of a spherical bubble of diameter d. Let us define the total volumetric interfacial area by:

$$a_i \equiv \int_\Omega \pi d^2 f \, \mathrm{d}(d) \tag{57}$$

and the averaged velocity transporting this volumetric interfacial area, which is the centre of area velocity, by:

$$\vec{V}_i \equiv \frac{\int_\Omega \dot{x} \pi d^2 f \, \mathrm{d}(d)}{\int_\Omega \pi d^2 f \, \mathrm{d}(d)} \tag{58}$$

The volumetric interfacial area source term corresponding to the bubble number density variation is defined by:

$$S_{\text{number}} = \int_\Omega \pi d^2 h \, \mathrm{d}(d) \tag{59}$$

and the source term induced by the size variation of the existing bubbles is defined by:

$$S_{\text{size}} = \int_\Omega \frac{\mathrm{d}A}{\mathrm{d}t} f \, \mathrm{d}(d) \tag{60}$$

Considering the above definitions, the volumetric interfacial area transport equation can be obtained from Eq. (52) by taking $\psi = \pi d^2$. We obtain:

$$\frac{\partial a_i}{\partial t} + \mathrm{div}(a_i \vec{V}_i) = S_{\text{number}} + S_{\text{size}} \tag{61}$$

In what follows, we will examine separately the two terms S_{number} and S_{size}.

3.2.2.1. Source term induced by nucleation. The nucleation effect is contained into the term S_{number}. If we assume that all the nucleated bubbles appear with the same diameter d_{nuc}, the function h will take the form:

$$h = \phi_n^{\text{NUC}} \delta(d - d_{\text{nuc}}) \tag{62}$$

where δ is the Dirac distribution. Using Eq. (59), the total volumetric interfacial area source term induced by nucleation is:

$$S_{\text{nuc}} = \pi d_{\text{nuc}}^2 \phi_n^{\text{NUC}} \tag{63}$$

Considering also coalescence and breakup effect, the total contribution of the bubble number density variations to the volumetric interfacial area can be expressed as:

$$S_{\text{number}} = \pi d_{\text{nuc}}^2 \phi_n^{\text{NUC}} + \frac{36\pi}{3} \left(\frac{\alpha}{a_i} \right)^2 (\phi_n^{\text{CO}} + \phi_n^{\text{BK}}) \tag{64}$$

3.2.2.2. Source term induced by the size variation of the existing bubbles. Let us consider a single bubble with a diameter d, the time variations of its volume and its external surface area can be related to the time variation of its diameter, due to the sphericity assumption:

$$\frac{\mathrm{d}V}{\mathrm{d}t} = \frac{\pi d^2}{2} \frac{\mathrm{d}(d)}{\mathrm{d}t}, \quad \frac{\mathrm{d}A}{\mathrm{d}t} = 2\pi d \frac{\mathrm{d}(d)}{\mathrm{d}t} \tag{65}$$

In addition, we have:

$$\frac{\mathrm{d}V}{\mathrm{d}t} = \frac{\mathrm{d}}{\mathrm{d}t} \left(\frac{m}{\rho_g} \right) = \frac{\dot{m}}{\rho_g} - \frac{V}{\rho_g} \frac{\mathrm{d}\rho_g}{\mathrm{d}t} \tag{66}$$

The first term in the RHS of Eq. (66) corresponds to the mass flux through the bubble surface, and the second term corresponds to the compressibility and thermal inflation.

The mass flux through the bubble surface can be expressed by:

$$\dot{m} = -\frac{q_1'' + q_2''}{L} A \tag{67}$$

where q_1'' and q_2'' are the heat flux densities between each phase and the interface and L is the latent heat of vaporisation.

Accordingly, from the above equations, we have:

$$\frac{\mathrm{d}A}{\mathrm{d}t} = \frac{4}{d\rho_g} \left(-\frac{q_1'' + q_2''}{L} A - V \frac{\mathrm{d}\rho_g}{\mathrm{d}t} \right) \tag{68}$$

It should be noted from the above equation that the contribution of the bubble to the volumetric interfacial area depends on its diameter. Generally speaking, the diameter pdf is needed to determine the total changes in the volumetric interfacial area induced by the bubble size variations for all the existing bubbles. Nevertheless, the complete closure of the Liouville equation and the numerical resolution of this equation is a rather difficult task, and is beyond the scope of this paper. Instead, we assume here a uniform bubble size for all the existing bubbles (except for the newly nucleated bubbles which are characterized by the diameter d_{nuc}) given by the Sauter mean diameter d_s. This implies the following form for the pdf:

$$f = n\delta(d - d_s) \tag{69}$$

We obtain, from the definition (60) and using Eqs. (68) and (69):

$$S_{\text{size}} = n \frac{4}{d_s \rho_g} \left(-\frac{q_1'' + q_2''}{L} A(d_s) - V(d_s) \frac{\mathrm{d}\rho_g}{\mathrm{d}t} \right) \tag{70}$$

Substituting n and d_s from Eqs. (42) and (43), the above equation can be rewritten into the following form:

$$S_{\text{size}} = \frac{2}{3} \frac{a_i}{\alpha \rho_g} \left(\Gamma_{g,i} - \alpha \frac{\mathrm{d}\rho_g}{\mathrm{d}t} \right) \tag{71}$$

where $\Gamma_{g,i}$ is the interfacial mass transfer through the surfaces of the existing bubbles, without nucleation.

In conclusion, the volumetric interfacial area transport equation is given by the following equation:

$$\frac{\partial a_i}{\partial t} + \mathrm{div}(a_i \vec{V}_i) = \frac{2}{3}\frac{a_i}{\alpha\rho_g}\left(\Gamma_{g,i} - \alpha\frac{d\rho_g}{dt}\right) + \frac{36\pi}{3}\left(\frac{\alpha}{a_i}\right)^2(\phi_n^{CO} + \phi_n^{BK}) + \pi d_{nuc}^2\phi_n^{NUC} \quad (72)$$

where the nucleated bubble diameter and source term will be described in the next section.

4. Presentation of the complete model we use for our calculations

The volumetric interfacial area balance equation we have presented in the previous sections is solved together with the mass, momentum and energy balance equations of the two-fluid model [1], and a K–ε model for the turbulence in the liquid phase. These equations and their closure relations are summarised below.

The six balance equations of our two-fluid model write [1,19]:

- Two mass balance equations:

$$\frac{\partial}{\partial t}(\alpha_k\rho_k) + \nabla\cdot(\alpha_k\rho_k\vec{V}_k) = \Gamma_k \quad (73)$$

where Γ_k is the volumetric production rate of phase k due to phase change (including nucleation).

- Two momentum balance equations:

$$\alpha_k\rho_k\frac{d_k\vec{V}_k}{dt} = \mathrm{div}[\alpha_k(\overleftrightarrow{t}_k + \overleftrightarrow{t}_k^{Re})] - \alpha_k\nabla P + \vec{M}_{ki} + \alpha_k\rho_k\vec{g} + \Gamma_k(\vec{V}_{ki} - \vec{V}_k) \quad (74)$$

where the first term in the RHS contains the molecular stress tensor and the turbulent Reynolds stress tensor. The closure of the Reynolds stress tensor for the liquid phase will be described in the following, together with the closure of the averaged interfacial momentum transfer term M_{ki}. It should be noted that we neglect the Reynolds stress tensor for the dispersed gaseous phase.

- Two internal energy balance equations:

$$\frac{\partial}{\partial t}(\alpha_k\rho_k e_k) + \nabla\cdot(\alpha_k\rho_k e_k\vec{V}_k) = \nabla\cdot\left[\alpha_k\left(\lambda_k\nabla T_k + \frac{\rho_k\nu_{tk}}{Pr_t}\nabla e_k\right)\right] - P\left[\frac{\partial\alpha_k}{\partial t} + \nabla\cdot(\alpha_k\vec{V}_k)\right] + \Gamma_k H_{ki} + q_{ki} \quad (75)$$

where we have written separately the molecular conduction and the turbulent diffusion, ν_{tk} being the turbulent viscosity for phase k, H_{ki} is the mean enthalpy of phase k near interfaces, and q_{ki} is the interfacial heat flux. The modeling of q_{ki} will be presented in the following.

- Liquid turbulence K–ε equations:

In addition to the six above balance equations, and to Eq. (72) for the volumetric interfacial area, we also use a K–ε turbulence model for the liquid phase, which includes the effect of the bubble induced turbulence [19,20]. The two balance equations for the turbulent kinetic energy and for its dissipation rate write:

$$\frac{\partial}{\partial t}(\alpha_l\rho_l K_l) + \nabla\cdot(\alpha_l\rho_l K_l\vec{V}_l) = \nabla\cdot\left(\alpha_l\rho_l\frac{\nu_{tl}}{Pr_{tK}}\nabla K_l\right) - \alpha_l\rho_l\varepsilon_l + \alpha_l\overleftrightarrow{t}_l^{Re} : \nabla\vec{V}_l + P_K^i - \sigma(\phi_{a_i}^{RC} + \phi_{a_i}^{TI}) + K_{li}\Gamma_l \quad (76)$$

$$\frac{\partial}{\partial t}(\alpha_l\rho_l\varepsilon_l) + \nabla\cdot(\alpha_l\rho_l\varepsilon_l\vec{V}_l) = \nabla\cdot\left(\alpha_l\rho_l\frac{\nu_{tl}}{Pr_\varepsilon}\nabla\varepsilon_l\right) - C_{\varepsilon 2}\alpha_l\rho_l\frac{\varepsilon_l^2}{K_l} + C_{\varepsilon 1}\frac{\varepsilon_l}{K_l}\alpha_l\overleftrightarrow{t}_l^{Re} : \nabla\vec{V}_l - \frac{2}{3}\alpha_l\rho_l\varepsilon_l\nabla\cdot\vec{V}_l + P_\varepsilon^i + \varepsilon_{li}\Gamma_l \quad (77)$$

where the fifth term in the RHS of Eq. (76) corresponds to the energy exchange between the interfacial free energy and the liquid turbulent kinetic energy due to the bubbles coalescence and breakup. In these equations, the liquid Reynolds stress tensor and the liquid turbulent eddy viscosity are assumed to be given by the following relations:

$$\overleftrightarrow{t}_l^{Re} \triangleq -\rho_l\overline{\vec{u}'\vec{u}'}^l = \rho_l\nu_{tl}(\nabla\vec{V}_l + \nabla^T\vec{V}_l) - \frac{2}{3}\rho_l(K_l + \nu_{tl}\nabla\cdot\vec{V}_l)\overleftrightarrow{I} \quad (78)$$

$$\nu_{tl} \triangleq C_\mu\frac{K_l^2}{\varepsilon_l} \quad (79)$$

The source terms corresponding to the turbulence produced in the wakes of bubbles are modeled according to [20–22]:

$$P_K^i = -(\vec{M}_g^D + \vec{M}_g^{MA})(\vec{V}_g - \vec{V}_l) \quad (80)$$

$$P_\varepsilon^i = C_{\varepsilon 3}\frac{P_K^i}{\tau}, \quad \tau = \left(\frac{d_s^2}{\varepsilon_l}\right)^{1/3} \quad (81)$$

where τ is a characteristic time for the bubble induced turbulence, and $\vec{M}_g^D$ and $\vec{M}_g^{MA}$ are the averaged drag and added mass forces exerted on the dispersed phase in the momentum equations.

In the above equations, the default values of the different coefficients are $Pr_t = 0.9$, $Pr_{tK} = 1$, $Pr_{t\varepsilon} = 1.3$, $C_{\varepsilon 1} = 1.44$, $C_{\varepsilon 2} = 1.92$, $C_\mu = 0.09$ [23]. The value of the constant $C_{\varepsilon 3}$ is equal to 1 for calculations of the DEDALE experiment and has been adjusted to 0.6 for calculations of the DEBORA experiment [24].

4.1. Interfacial momentum transfer closure laws

The interfacial momentum transfer term is assumed to be the sum of four different contributions [19,25]:

$$\vec{M}_{ki} = \vec{M}_k^{D} + \vec{M}_k^{MA} + \vec{M}_k^{L} + \vec{M}_k^{DT} \tag{82}$$

where the four terms in the RHS of (82) are given by the following relations.

- Drag force:

$$\vec{M}_g^{D} = -\vec{M}_l^{D} = -\frac{1}{8} a_i \rho_l C_D |\vec{V}_g - \vec{V}_l| (\vec{V}_g - \vec{V}_l) \tag{83}$$

where C_D is the drag coefficient. This coefficient is expressed according to Ishii [1,26].

- Added mass force:

$$\begin{aligned} \vec{M}_g^{MA} &= -\vec{M}_l^{MA} \\ &= -C_{MA} E(\alpha) \alpha \rho_l \left[\left(\frac{\partial \vec{V}_g}{\partial t} + \vec{V}_g \cdot \nabla \vec{V}_g \right) \right. \\ &\quad \left. - \left(\frac{\partial \vec{V}_l}{\partial t} + \vec{V}_l \cdot \nabla \vec{V}_l \right) \right] \end{aligned} \tag{84}$$

where the factor $E(\alpha)$ takes into account the effect of the surrounding bubbles, it is given by [27]:

$$E(\alpha) = \frac{1 + 2\alpha}{1 - \alpha} \tag{85}$$

- Lift force:

$$\begin{aligned} \vec{M}_g^{L} &= -\vec{M}_l^{L} \\ &= -C_L \alpha \rho_l (\vec{V}_g - \vec{V}_l) \cdot (\nabla \vec{V}_l - \nabla^T \vec{V}_l) \end{aligned} \tag{86}$$

- Turbulent bubble dispersion force:

$$\vec{M}_g^{DT} = -\vec{M}_l^{DT} = -C_{DT} \rho_l K_l \nabla \alpha \tag{87}$$

The default values of the coefficients retained in our calculations are $C_{MA} = 0.5$, $C_L = 0.5$ [28]. The coefficient C_{DT} is equal to 1 for calculations of the DEDALE experiment and has been adjusted to 2.5 for calculations of the DEBORA experiment.

4.2. Interfacial heat transfer closure laws [29,30]

- For the interface to liquid heat transfer, we have:

$$q_{li} = h_{li} a_i (T_{sat} - T_l) \quad \text{and} \quad h_{li} = \frac{\lambda_l}{d_s} Nu \tag{88}$$

where h_{li} is the heat transfer coefficient between the liquid and the interface and Nu is the Nusselt number. In the case of condensation ($Ja \leqslant 0$), we have for the Nusselt number:

$$Nu = 2 + 0.6 Re^{0.5} Pr^{0.33} \tag{89}$$

while in the case of evaporation ($Ja \geqslant 0$), the Nusselt number is given by:

$$Nu = \mathrm{Max}(Nu_1, Nu_2, Nu_3) \tag{90}$$

where the three Nusselt numbers in the RHS of (90) are modeled according to [29,30]:

$$Nu_1 = \sqrt{\frac{4Pe}{\pi}}, \quad Nu_2 = \frac{12}{\pi} Ja, \quad Nu_3 = 2 \tag{91}$$

with the following definitions for the Jakob, Reynolds and Péclet numbers:

$$Ja = \frac{\rho_l C_{pl} (T_l - T_{sat})}{\rho_g L}, \quad Re = \frac{d_s U_r}{\nu_l}, \quad Pe = \frac{d_s U_r}{a_l} \tag{92}$$

where L is the latent heat of vaporisation and U_r is the norm of the relative velocity between phases.

- The interface to vapour heat transfer is expressed in the following manner:

$$q_{gi} = \frac{\alpha \rho_g C_{pg}}{\delta t} (T_{sat} - T_g) \tag{93}$$

where δt is the numerical time step. This expression guarantees that the vapour temperature is very close to the saturation temperature.

4.3. Wall heat transfer

The wall-to-liquid heat flux can be divided into three parts [29]:

$$q_w = q_c + q_q + q_e \tag{94}$$

- The first part is the "single phase" like heat transfer through the contact area A_c between the liquid and the duct wall:

$$q_c = A_c h_{log} (T_w - T_l) \tag{95}$$

where the heat transfer coefficient is expressed by:

$$h_{log} = \rho_l C_{pl} \frac{u^*}{T^+} \tag{96}$$

In this expression, u^* is the wall friction velocity and T^+ is the non-dimensional temperature in the wall

boundary layer. Classical expressions for these two quantities can be found in [23].

- The second part is the heat flux due to the quenching effect:

$$q_q = A_q t_q f \frac{2\lambda_l (T_w - T_l)}{\sqrt{\pi a_l t_q}} \quad (97)$$

where A_q, t_q, f and a_l are the fraction of the wall area occupied by the nucleated bubbles, the time delay between the detachment of one bubble and the apparition of the following one, the detachment frequency of the nucleated bubbles and the thermal diffusivity of the liquid. The quantities A_q, t_q and f are modeled as functions of the active nucleation site density N and the bubble detachment diameter d_{nuc} [29].

- The third part is the heat flux used for phase change (bubbles nucleated on the wall surface):

$$q_e = f \frac{\pi}{6} d_{nuc}^3 \rho_g L N \quad (98)$$

In these relations, the bubble detachment diameter d_{nuc} is given by Ünal [31] and Borée et al. [32] and the correlation for the active nucleation site density N given by Kurul and Podowski [33] has been used in our calculations. The bubble detachment diameter d_{nuc} has also been used as the newly nucleated bubble diameter d_{nuc} in the volumetric interfacial area balance equation (72).

5. Simulations of the DEBORA experiment with four different interfacial area models

5.1. Description of the DEBORA experiment

The DEBORA experiment, which was carried at the *Commissariat à l'Energie Atomique* [29], has been chosen to evaluate our model. In this experiment, the R-12 has been adopted as the working fluid to simulate the pressurized water reactor conditions under low pressure. Some liquid R-12 flows upwardly inside a vertical pipe having an internal diameter equal to 19.2 mm. The whole pipe can be divided axially into three parts: the adiabatic inlet section (1 m length), the heated section (3.5 m length) and the adiabatic outlet section (≈0.5 m length). Vapour bubbles are generated by nucleation onto the wall surface, and condense into the subcooled liquid when they are far from the wall. At the end of the heated section, the radial profiles of the void fraction and bubble diameter have been measured by means of an optical probe and the liquid temperature has been measured by means of thermocouples. The three-dimensional module of the CATHARE code [34] has been used for the numerical calculations. A cylindrical axisymmetrical meshing, having 80 meshes in the axial direction and 10 meshes in the radial direction, has been used. Four different DEBORA test cases have been simulated, these tests are listed in Table 2. The measurement uncertainties were evaluated by Manon [29] to be ±0.02 on the void fraction, ±10% on the volumetric interfacial area and ±12% on the Sauter mean diameter. We have also noted an uncertainty on the liquid temperature equal to ±0.2 °C on Manon's figures for the tests DEB5 and DEB6.

5.2. Comparisons of the calculation results to the experimental data

We made calculations of the four DEBORA test cases indicated in Table 2 with five different models for the interfacial configuration:

- We can impose the radial profile of the bubble diameter *measured in the experiment* and deduce the volumetric interfacial area from the calculated void fraction and from this experimental bubble diameter profile by using Eq. (42). In this case, the volumetric interfacial area balance equation is not used. These calculations are indicated by solid lines in Figs. 1–4. The four other models use the volumetric interfacial area balance equation (72) with different models for the turbulent coalescence and breakup terms.
- Wu's model [2] for the coalescence and breakup terms has been used. The corresponding calculations are indicated by dotted lines in Figs. 1–4.
- Hibiki and Ishii's model [5] for the coalescence and breakup terms has been used. The corresponding calculations are indicated by dashed lines in Figs. 1–4.
- Ishii and Kim's model [6] for the coalescence and breakup terms has been used. The corresponding calculations are indicated by long dashed lines in Figs. 1–4.

Table 2
DEBORA selected test cases and their experimental conditions

Case no.	Pressure (bar)	Mass flow rate (kg/m^2/s)	Wall heat flux density (kW/m^2)	Inlet temperature (°C)	Saturation temperature (°C)	Outlet vapour quality
DEB5	26.15	1986	73.89	68.52	86.64	0.0580
DEB6	26.15	1984.9	73.89	70.53	86.64	0.0848
DEB10	14.59	2027.8	76.24	34.91	58.15	0.0261
DEB13	26.17	2980.9	109.42	69.20	86.64	0.0621

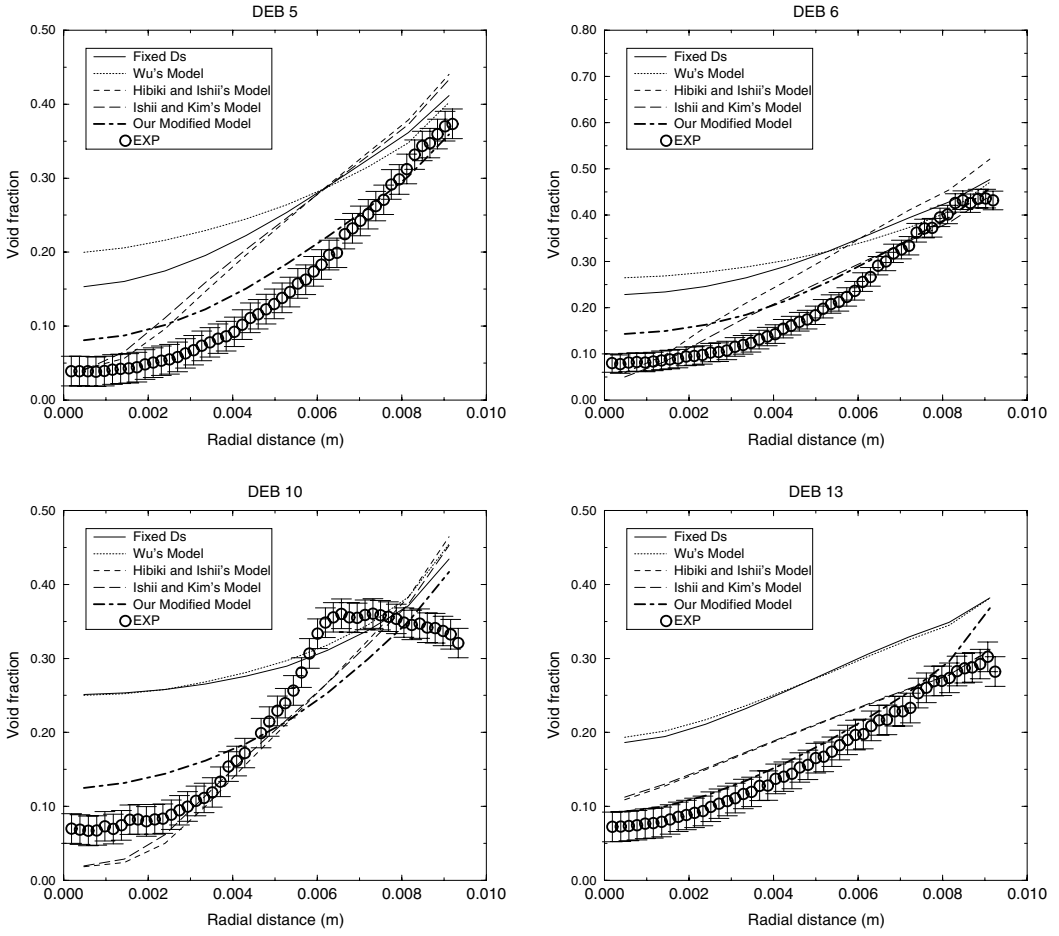

Fig. 1. Comparison between the DEBORA experimental data and the results of four different models for the void fraction at the end of the heated section.

- For the last type of calculations, we use our models for the coalescence (Eq. (22)) and breakup (Eq. (37)) terms. These calculations are indicated by dot-dashed thick lines in Figs. 1–4.

The results of the five types of calculations are presented together with the experimental measurements (indicated by circles) in Figs. 1–4, for the four test cases indicated in Table 2. In each figure, four graphs corresponding to the test cases DEB5, DEB6, DEB10 and DEB13 are presented. The comparison of the void fraction profiles is presented in Fig. 1, whereas the results on the liquid temperature are presented in Fig. 2. The comparison of the geometrical parameters, namely the mean bubble diameter and the volumetric interfacial area, are presented in Figs. 3 and 4 respectively. The experimental uncertainties are also indicated by vertical segments on these figures.

First, it can be seen in Fig. 1 that the void fraction is generally overestimated by the code, especially in the core of the duct. Except for the test DEB10, where Hibiki and Kim models [5,6] both underestimate the void fraction in the core of the flow, the void fraction is generally over-predicted by the code, whatever the model used and especially for the calculations where we have imposed the experimentally measured bubble diameter profile. This observation shows that the over-prediction of the void fraction comes from the uncertainties concerning the heat and mass transfer models, rather than the interfacial area models. The comparison of the liquid temperature profiles for the two test cases where the experimental profile was available (DEB5 and DEB6) is presented in Fig. 2. One can see that the liquid temperature is generally overestimated by the code near the wall. It is also underestimated in the core of the flow for the models derived by Hibiki and Kim [5,6] and for our model. The three calculations with low values of the liquid temperature in the core of the duct, give also the lower values of the void fraction in this region. This is due to the fact that the interface to liquid heat flux is

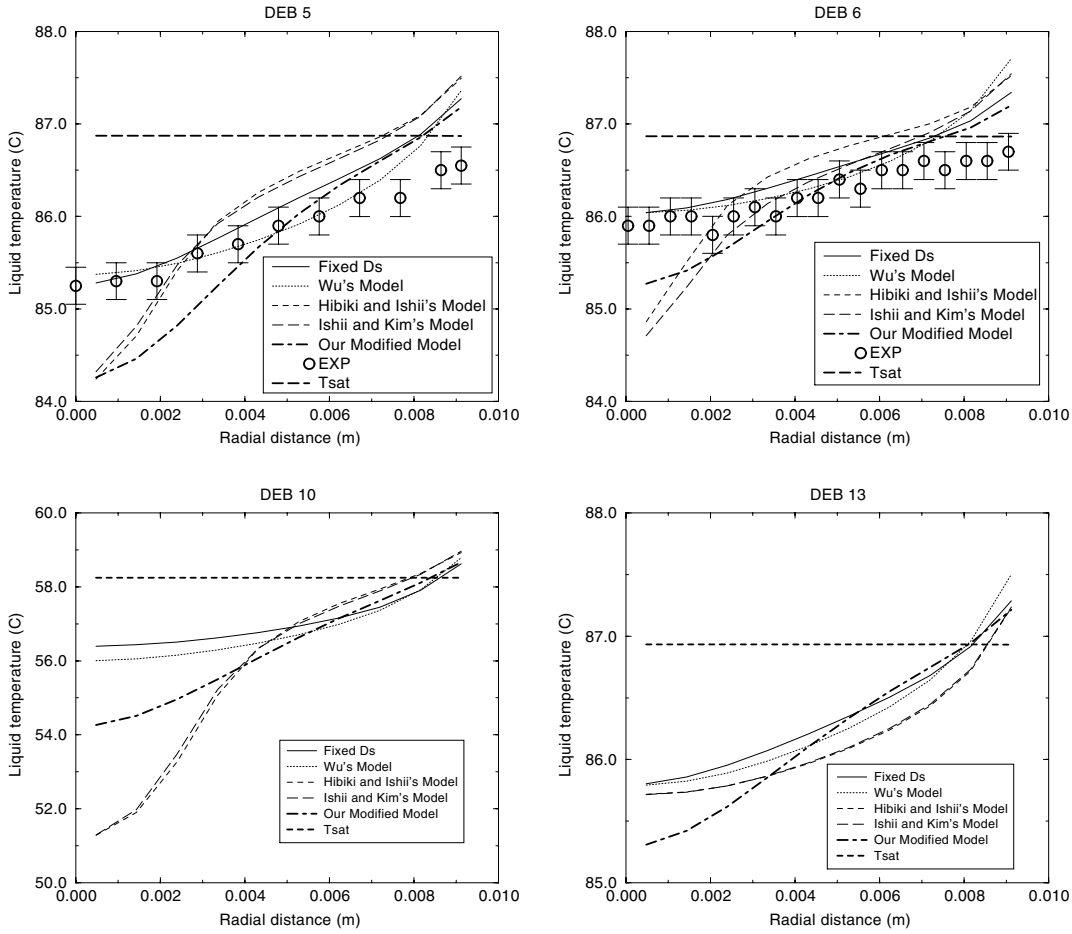

Fig. 2. Comparison between the DEBORA experimental data and the results of four different models for the liquid temperature at the end of the heated section.

more important when the liquid temperature is lower, in comparison to the saturation temperature, therefore giving more phase change by condensation.

Fig. 3 shows that the best agreement on the bubble diameter profiles is generally obtained with our model. Wu's model [2] gives generally a strong overestimation of the bubble diameter. Among the four models tested, Wu's model has been derived the first and it appears later that an error has been introduced in the derivation of the wake entrainment induced bubble coalescence [6,7]. In addition, the gas expansion term corresponding to the first term in the RHS of Eq. (1) was not retained in Wu's model. As pointed out by [6,7], this term is not negligible in upward adiabatic bubbly flow of air/water at atmospheric pressure, and is certainly not negligible in heated boiling flow. The two other models [5,6] give better values for the magnitude of the bubble diameter, but not the good shape of the radial profiles. Our model is the only one that gives the good shape for the bubble diameter profiles (Fig. 3). The reason of this have been partly discussed in the previous sections. We believe that the main advantage of our model, in comparison to the other models tested on DEBORA, is that we have decomposed the times necessary for breakup or coalescence into two contributions: free travelling time between two collisions and interaction time between bubbles or between a bubble and an eddy after collision. The bubble oscillation resonance mechanism has been considered for turbulent breakup, and the second mode bubble oscillation period has been retained for the bubble breaking time. In addition, the numerical constants appearing in the models other than ours have been fitted on adiabatic air/water experiments, and their validity for boiling R-12 is questionable. Instead, the numerical coefficients appearing in our model have been calculated theoretically, and it seems to give quite good results for the bubble diameter in our DEBORA calculations.

Fig. 4 shows the comparison of the volumetric interfacial area profiles. Our model generally overestimates

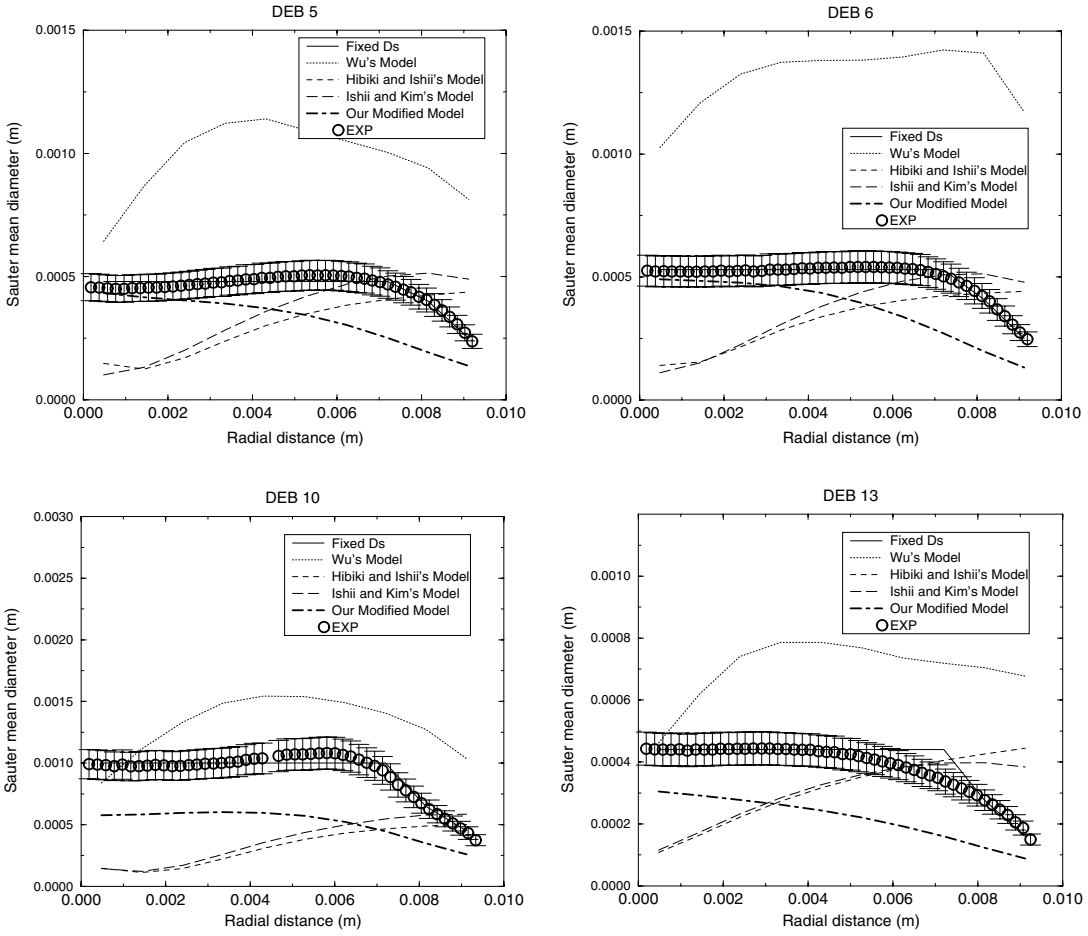

Fig. 3. Comparison between the DEBORA experimental data and the results of four different models for the mean bubble diameter at the end of the heated section.

the volumetric interfacial area, especially near the wall. We recall that the volumetric interfacial area, the void fraction and the mean bubble diameter are related by Eq. (42). The overestimation of the volumetric interfacial area is coherent with the underestimation of the bubble diameter (Fig. 3) and with the overestimation of the void fraction for the tests DEB10 and DEB13 (Fig. 1).

6. Simulations of the DEDALE experiment with four different interfacial area models

6.1. Description of the DEDALE experiment

In the preceding section, we have shown that our model for bubble diameter prediction give quite good results on the DEBORA experiment, in comparison to three other models of the literature [2,5,6]. The numerical constants appearing in our model have been derived theoretically. The numerical constants in the models derived by other authors [2,5,6] were partly fitted on air/water adiabatic bubbly flow experiments. This could partly explain why we have obtained better results on the bubble diameter profile in the calculations of the DEBORA experiment, in comparison to the three other models. The other models being fitted on air/water adiabatic bubbly flows, we have chosen such an experiment to compare our model to the other ones. We have chosen the DEDALE experiment which was carried at Electricité de France [35,36]. The subject of this experiment was the investigation of the axial development of adiabatic air/water bubbly and bubbly-to-slug transition flows in a vertical pipe. The test section was 6 m long and 38.1 mm of internal diameter. The working fluids were water and air under atmospheric pressure, and no heating was imposed in this experiment. The DEDALE experiment is quite similar to the experiments used by the other authors [2,5,6] to fit the constants in their

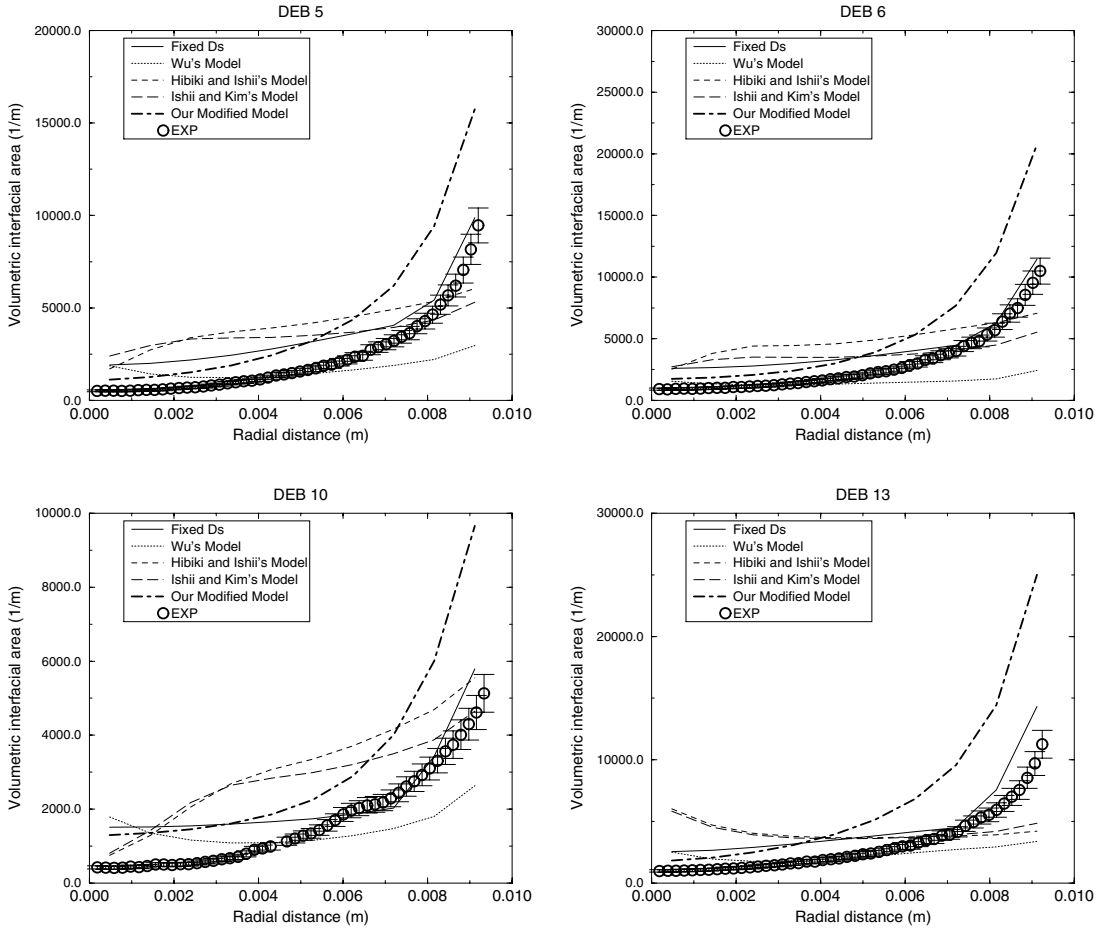

Fig. 4. Comparison between the DEBORA experimental data and the results of four different models for the volumetric interfacial area at the end of the heated section.

models. Radial profiles of the void fraction, volumetric interfacial area, mean bubble equivalent diameter, mean liquid and gas velocities and axial liquid turbulent random mean square (r.m.s.) velocity were measured at three different elevations, located at 8, 55 and 155 diameters from the inlet. The measurements in the first measuring section ($Z/D = 8$) were used as inlet boundary conditions for our simulations. We can compare the results of our simulations to the experimental results in the two other measuring sections ($Z/D = 55$ and 155). Two different tests have been retained for our calculations, the inlet liquid and gas superficial velocities for these two tests being given in Table 3.

We have no direct information about uncertainties for the local measurements. Nevertheless, the author made some coherency test between local quantities and global ones by integrating the local quantities over the tube cross-section or its diameter and comparing the obtained averaged quantities to global ones obtained by different measurement methods. The time-averaged local void fraction obtained by an optical double sensor probe was integrated on the duct diameter and compared to the line (and time) averaged void fraction on the same diameter obtained from gamma densitometry measurement. The time-averaged local gas velocity, also measured with the double sensor probe, allows to calculate the local gas volumetric flux j_g. This local gas volumetric flux was integrated on the duct cross-section and compared to the area (and time) averaged gas volumetric flux J_g obtained by a mass flow controller. The same

Table 3
DEDALE selected test cases and corresponding inlet superficial velocities

DEDALE no.	J_l (m/s)	J_g (m/s)
1101	0.877	0.0588
1103	0.877	0.1851

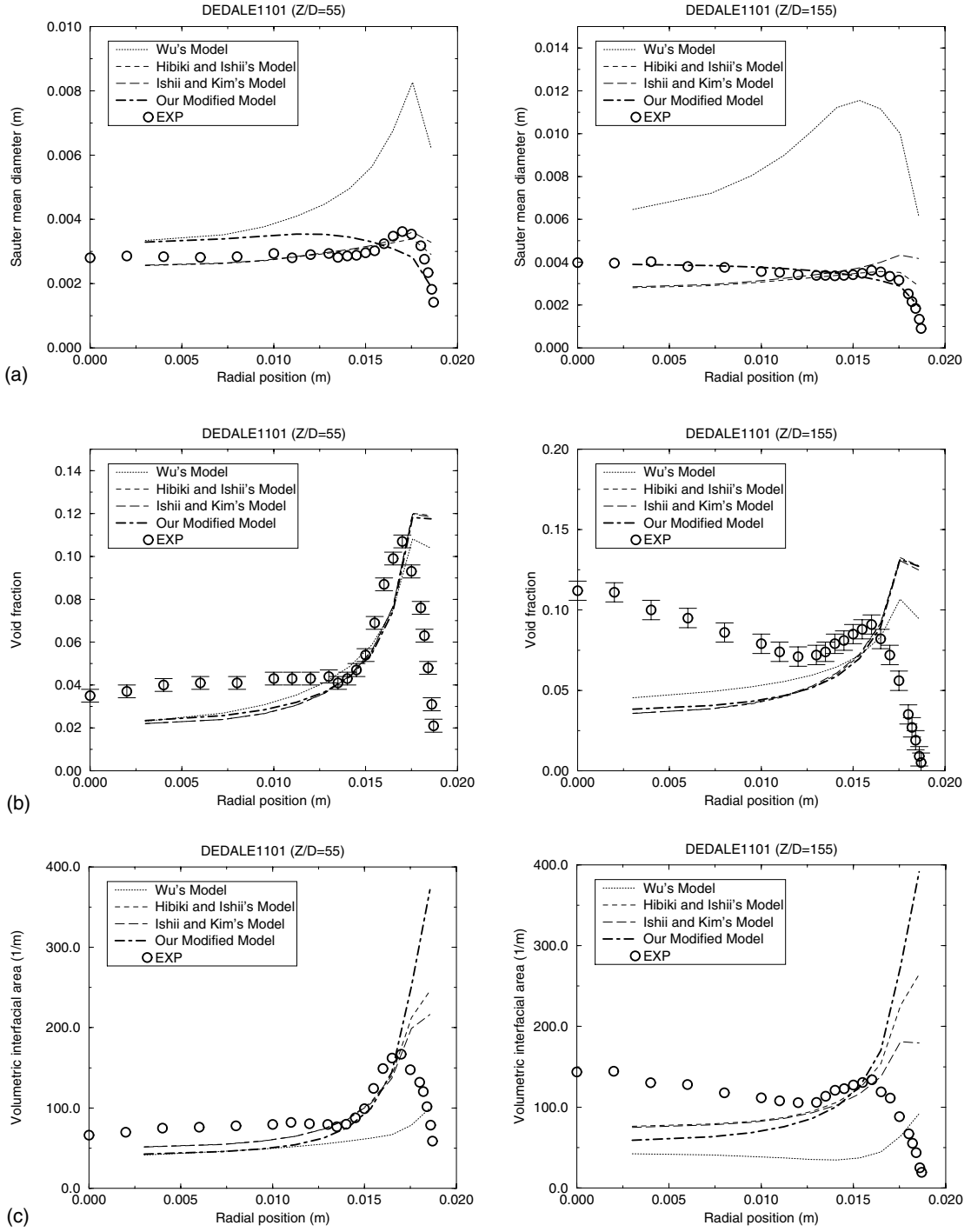

Fig. 5. Comparison between the DEDALE experimental data and the results of four different models at two different elevations for the test 1101. Profiles of bubble diameter (a), void fraction (b), volumetric interfacial area (c), the gas phase velocity (d), liquid phase velocity (e) and turbulence intensity (f).

procedure is applied to check the coherency of the liquid volumetric fluxes j_l and J_l, the time-averaged local liquid velocity being measured by hot-film anemometry and the mean liquid volumetric flux being measured by an

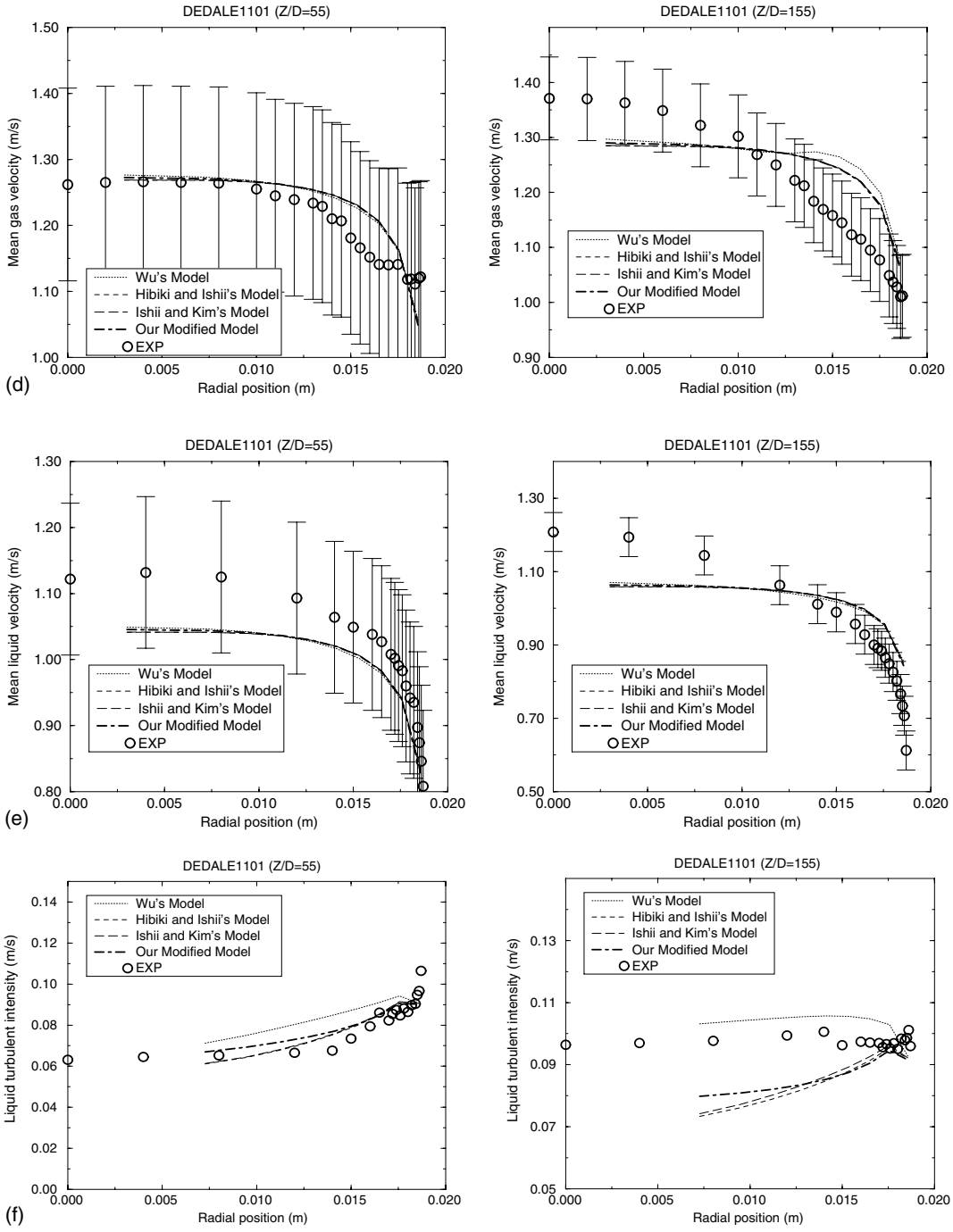

Fig. 5 (*continued*)

electromagnetic flow-meter. The differences between $\langle\alpha\rangle$ and α_{gamma}, between $\langle j_{\text{l}}\rangle$ and J_{l} and between $\langle j_{\text{g}}\rangle$ and J_{g} were indicated by the author for each measuring section for the test 1101. Taking these differences as uncertainties, we have deduced the uncertainties on the mean liquid and gas velocities by making the simplifying assumption that local quantities does not vary in the cross-section (which is a strong approximation for α). These evaluated uncertainties are indicated by vertical segments in Fig. 5b, d and e. We have no enough infor-

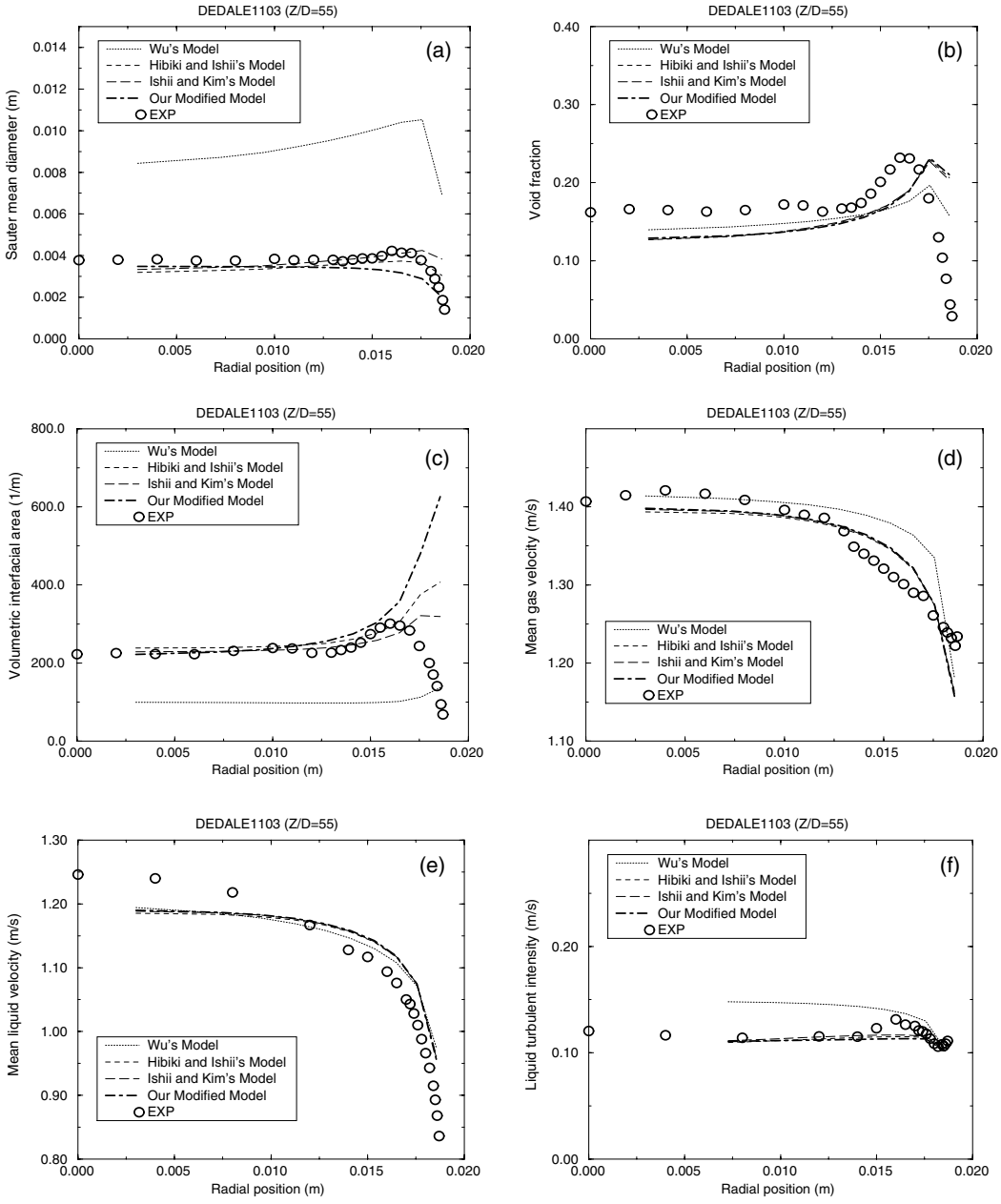

Fig. 6. Comparison between the DEDALE experimental data and the results of four different models at $Z/D = 55$ for the test 1103. Profiles of bubble diameter (a), void fraction (b), volumetric interfacial area (c), mean gas velocity (d), mean liquid velocity (e) and liquid turbulent intensity (f).

mation to estimate the uncertainties on the other quantities (a_i, d_s, u_l') or for the test 1103.

6.2. Comparisons of the calculations results to the experimental data

The comparisons of the radial profiles of the measured quantities at $Z/D = 55$ for the two tests and $Z/D = 155$ for the test 1101, with the calculated ones are presented onto Figs. 5 and 6. Experimental results show that the test 1103 is a bubbly flow at the elevation $Z/D = 55$ but a slug flow at the elevation $Z/D = 155$. As our model does not apply to slug flows, the comparison has been made only at the elevation $Z/D = 55$ for this test. In Figs. 5 and 6, the profiles of the mean bubble diameter (a), void fraction (b), volumetric interfacial

area (c), mean gas velocity (d), mean liquid velocity (e) and liquid turbulent intensity (f) are presented. In Fig. 5, the comparisons at the elevation $Z/D = 55$ are shown on the left column, and those at the elevation $Z/D = 155$ are shown on the right. For each test, we made four different calculations using Wu's model [2] (indicated by dotted lines on the figures), Hibiki's model [5] (indicated by dashed lines on the figures), Kim's model [6] (indicated by long dashed lines on the figures) and our model (indicated by dot-dashed lines on the figures).

The first test we have chosen (1101) is an upward bubbly flow up to the exit of the tube. However, due to the coalescence and gas expansion effects, the bubble size increases regularly along the tube as it can be seen by comparing the experimental values of the bubble diameter at the two different elevations (Fig. 5a). Due to this bubble size variation, the shape of the void fraction profile evolves along the tube. At the first comparing elevation ($Z/D = 55$), we observe a wall peaking void fraction profile, but at the second elevation ($Z/D = 155$), we observe an intermediate void fraction profile (intermediate between wall peaking and void coring) as it can be seen on Fig. 5b. The code qualitatively reproduces the wall peak of the void fraction at the first elevation, as a result of the equilibrium between the radial components of the lift force (Eq. (86)) and the turbulent dispersion force (Eq. (87)), but fails to reproduce the void fraction profile at the second elevation. The void fraction profiles obtained with the four different models for interfacial area prediction are quite similar, even if more important differences are visible on the bubble diameter and interfacial area profiles (Fig. 5a–c). The comparison of the bubble diameter profiles (Fig. 5a) shows that the better agreement is obtained with Hibiki's model and Kim's model [5,6] (which give quite similar results) at the first elevation ($Z/D = 55$), and with our model at the second elevation ($Z/D = 155$). The comparison of the mean and turbulent axial velocities (Fig. 5d–f) give quite similar results for the four different models. When the void fraction profile is qualitatively reproduced, as at the first elevation, the liquid turbulent intensity profile is also well reproduced with our K–ε model (Fig. 5f).

In the second test we have simulated (1103), a flow regime transition is observed experimentally between the elevation $Z/D = 55$, where a bubbly flow is observed, and the elevation $Z/D = 155$, where a slug flow is observed. As the different models we use are not able to describe slug flows, and the experimental measurements conducted by Grossetête were done by means of a double sensor probe for the dispersed phase, assuming spherical bubbles [35,36], we will only discuss the results obtained at the elevation $Z/D = 55$. As for the test 1101, the void fraction profile is qualitatively reproduced at the first elevation, for all the models tested. The mean bubble diameter is also well reproduced by the different models, except for Wu's model [2] which strongly overestimates the bubble diameter (Fig. 6a). The liquid turbulent r.m.s. velocity is also well predicted at the first elevation, as it can be seen in Fig. 6f.

7. Conclusions

In this paper, new models are proposed for the different source terms appearing in the RHS of the volumetric interfacial area balance equation for bubbly flows. These source terms correspond to the turbulence induced coalescence and breakup phenomena, as well as the gas expansion and phase change terms, including the nucleation of new bubbles on a heated wall. Our model has been tested in comparison to three other models for the coalescence and breakup terms found in the literature, on two different experiments. All the calculations were done with our formulation for the gas expansion term and for the phase change terms (Eq. (72)) because only this formulation allows to introduce a nucleated bubble diameter which is different from the Sauter mean diameter. The first experiment we have investigated is the DEBORA experiment, carried at the *Commissariat à l'Energie Atomique*, France. In this experiment, initially subcooled liquid R-12 is flowing upward in a vertical pipe with a heated wall. Some vapour bubbles are nucleated onto the wall surface, and after then migrate towards the core of the flow where they condense in colder liquid. The comparisons of the radial profiles of the void fraction, liquid temperature, mean bubble diameter and interfacial area at the end of the heated section show a better agreement with our model than with the three other models. We believe that one reason of this is that we have separately considered the "free travelling time" and the "interaction time" in the modeling of the bubbles coalescence and breakup, as is explained in Sections 1 and 2. Another reason may be that the numerical constants appearing in the models derived by the other authors were fitted onto adiabatic air/water experiments, and that their validity for boiling R-12 experiment is questionable. Instead, the numerical constants appearing in our model were derived theoretically, and therefore we hope that the range of applicability of our model is less restricted in terms of fluids and working conditions. In order to verify this assertion, we have also compared the four models predictions to the DEDALE experiment which is an adiabatic air/water experiment. When the flow is in the bubbly regime, the prediction of the mean bubble diameter is quite good for Hibiki's model [5] and Kim's model [6], as well as for our model. The liquid turbulent r.m.s. velocity is also well predicted.

Because the DEBORA experimental data base is only concerned with subcooled boiling, our model has not been tested in the case of saturated boiling. The application of our model to saturated boiling conditions will

be addressed in future work. In theory, our model should be applicable to void fraction values as elevated as α_{max} given by Eq. (12). In practice, when the void fraction is increased, a transition from bubbly-to-slug flow may be observed, depending on the flow conditions. The gas plugs being of the same size than the tube internal diameter, the assumptions made to derive the turbulent coalescence and breakup terms are clearly not valid for a slug flow. One should speak of limiting bubble size, rather than void fraction, for our model to be applicable.

Further research is needed for bubbly flow configurations were several bubble size are present simultaneously in a small volume (multidispersed bubbly flow) for a better prediction of the transition from bubbly-to-slug flow, or for reproducing intermediate void fraction profile, as the one observed at the higher measuring section in DEDALE 1101 (Fig. 5b). In a recent approach, Hibiki and Ishii [37] tried to predict the transition from bubbly-to-slug flow by using a "two group model" involving separate balance equations for the void fractions and the interfacial areas of small spherical or distorted bubbles, and for big cap bubbles or slugs.

Acknowledgements

The authors are fully indebted to the Commissariat à l'Energie Atomique of France, to Electricité de France and also to FRAMATOME and to the French Institute for Nuclear Safety for their financial support in the context of the NEPTUNE project.

References

[1] M. Ishii, Two-fluid model for two-phase flow, Multiphase Sci. Technol. 5 (1990) 1–58.
[2] Q. Wu, S. Kim, M. Ishii, S.G. Beus, One-group interfacial area transport in vertical bubble flow, Int. J. Heat Mass Transfer 41 (8–9) (1998) 1103–1112.
[3] C.W. Stewart, Bubble interaction in low-viscosity liquids, Int. J. Multiphase Flow 21 (6) (1995) 1037–1046.
[4] T. Otake, S. Tone, K. Nakao, Y. Mitsuhashi, Coalescence and breakup of bubbles in liquids, Chem. Eng. Sci. 32 (1977) 377–383.
[5] T. Hibiki, M. Ishii, One-group interfacial area transport of bubbly flows in vertical round tubes, Int. J. Heat Mass Transfer 43 (2000) 2711–2726.
[6] M. Ishii, S. Kim, Micro four-sensor probe measurement of interfacial area transport for bubbly flow in round pipes, Nucl. Eng. Des. 205 (2001) 2711–2726.
[7] J.M. Delhaye, Some issues related to the modelling of interfacial areas in gas–liquid flows, Part II: modelling the source terms for dispersed flows, C.R. Acad. Sci. Paris, Sér. IIb t. 329 (2001) 473–486.
[8] A.N. Kolmogorov, On the disintegration of drops in a turbulent flow, Doklady Akad. Nauk., SSSR 66 (1949) 825.
[9] F. Risso, The mechanisms of deformation and breakup of drops and bubbles, Multiphase Sci. Technol. 12 (2000) 1–50.
[10] C.A. Coulaloglou, L.L. Tavlaridès, Description of interaction processes in agitated liquid–liquid dispersions, Chem. Eng. Sci. 32 (1977) 1289–1297.
[11] G. Kocamustafaogullari, M. Ishii, Interfacial area and nucleation site density in boiling systems, Int. J. Heat Mass Transfer 26 (9) (1983) 1377–1387.
[12] M.J. Prince, H.W. Blanch, Bubble coalescence and breakup in air-sparged bubble columns, AIChE J. 36 (10) (1990) 1485–1499.
[13] R.D. Kirkpatrick, M.J. Lockett, The influence of approach velocity on bubble coalescence, Chem. Eng. Sci. 29 (1974) 2363.
[14] W.K. Kim, K.L. Lee, Coalescence behavior of two bubbles in stagnant liquids, J. Chem. Eng., Jpn. 20 (1987) 449.
[15] M. Sevik, S.H. Park, The splitting of drops and bubbles by turbulent fluid flow, J. Fluids Eng., Trans. ASME 53–60 (1973).
[16] D. Azbel, I.L. Athanasios, A mechanism of liquid entrainment, in: N. Cheremisinoff (Ed.), Handbook of Fluids in Motion, Ann Arbor Science Publishers, Ann Arbor, USA, 1983, p. 473.
[17] H. Lamb, Hydrodynamics, sixth ed., Dover Publications, New York, 1932.
[18] J.L. Achard, Contribution à l'étude théorique des écoulements diphasiques en régime transitoire, Ph.D. Thesis, Université Scientifique et Médicale, Institut National Polytechnique de Grenoble, 1978.
[19] C. Morel, Turbulence modeling and first numerical simulations in turbulent two-phase flows, in: 11th Symposium on Turbulent Shear Flows, vol. 3, Poster Session 3, Grenoble, France, September 8–10, 1997, pp. 3-10, 3-15.
[20] C. Morel, Modélisation multidimensionnelle des écoulements diphasiques gaz–liquide, Application à la simulation des écoulements à bulles ascendants en conduite verticale, Ph.D. Thesis, Ecole Centrale Paris, 1997.
[21] M. Lance, J.L. Marié, J. Bataille, Modélisation de la turbulence de la phase liquide dans un écoulement à bulles, La Houille Blanche No. 3/4, 1984.
[22] S.E. Elgobashi, T.W. Abou-Arab, A two-equation turbulence model for two-phase flows, Phys. Fluids 26 (4) (1983) 931–938.
[23] R. Schiestel, Modélisation et simulation des écoulements turbulents, Ed. Hermès, 1993.
[24] W. Yao, C. Morel, Prediction of parameters distribution of upward boiling two-phase flow with two-fluid models, in: 10th International Conference on Nuclear Engineering, Arlington, Virginia, USA, paper no. 22463, April 14–18, 2002.
[25] M. Lance, M. Lopez de Bertodano, Phase distribution phenomena and wall effects in bubbly two-phase flows, Multiphase Sci. Technol. 8 (1994) 69–123.
[26] M. Ishii, One-dimensional drift flux model and constitutive equations for relative motion between phases in various two-phase flow regimes, ANL Report No. 77-47, 1977.
[27] N. Zuber, On the dispersed two-phase flow in the laminar flow regime, Chem. Eng. Sci. 19 (1964) 897.
[28] T.R. Auton, The lift force on a spherical body in a rotational flow, J. Fluid. Mech. 183 (1987) 199–218.

[29] E. Manon, Contribution à l'analyse et à la modélisation locale des écoulements bouillants sous-saturés dans les conditions des réacteurs à eau sous pression, Ph.D. Thesis, Ecole Centrale Paris, 2000.
[30] P. Berne, Contribution à la modélisation du taux de production de vapeur par auto-vaporisation dans les écoulements diphasiques en conduites, Ph.D. Thesis, Ecole des Arts et Manufactures, 1983.
[31] H.C. Ünal, Maximum bubble diameter, maximum bubble-growth time and bubble-growth rate during the subcooled nucleate flow boiling, Int. J. Heat Mass Transfer 19 (1976) 643–649.
[32] J. Borée, G. Charnay, J. Fabre, D. Legendre, J. Magnaudet, Ecoulements diphasiques eau-vapeur avec changement de phase, Rapport IMFT-Interface, 1992.
[33] N. Kurul, M.Z. Podowski, Multidimensional effects in forced convection subcooled boiling, in: International Heat Transfer Conference, Jerusalem, vol. 1, Paper BO-04, 1991, pp. 31–45.
[34] F. Barré, C. Sun, I. Dor, Overview of the numerical and computational developments performed in the frame of the CATHARE 2 code, in: International Conference on Mathematics and Computations, Reactors Physics, and Environmental Analyses, Portland, Oregon, 30 April–4 May, 1995.
[35] C. Grossetête, Caractérisation expérimentale et simulation de l'évolution d'un écoulement diphasique à bulles ascendant dans une conduite verticale, Ph.D. Thesis, Ecole Centrale Paris, 1995.
[36] C. Grossetête, Experimental investigation and preliminary numerical simulations of void profile development in a vertical cylindrical pipe, in: A. Serizawa, T. Fukano, J. Bataille (Eds.), 2nd International Conference on Multiphase Flow, Kyoto, Japan, IF1-1-10, April 3–7, 1995.
[37] T. Hibiki, M. Ishii, Two-group interfacial area transport equations at bubbly-to-slug flow transitions, Nucl. Eng. Des. 202 (1) (2000) 39–76.